Scientia Iranica B (2023) 30(2), 454–463

Sharif University of Technology
Scientia Iranica
Transactions B: Mechanical Engineering
http://scientiairanica.sharif.edu

Research Note

Numerical appraisal of the unsteady Casson fluid flow through Finite Element Method (FEM)

M.M. Khader[a,b], M. Inc[c,d,*], and A. Akgul[e]

a. *Department of Mathematics and Statistics, College of Science, Imam Mohammad Ibn Saud Islamic University (IMSIU), Riyadh: 11566, Saudi Arabia.*
b. *Department of Mathematics, Faculty of Science, Benha University, Benha, Egypt.*
c. *Department of Mathematics, Faculty of Science, Firat University, 23119 Elazig, Turkey.*
d. *Department of Medical Research, China Medical University Hospital, China Medical University, Taichung, Taiwan.*
e. *Siirt University, Art and Science Faculty, Department of Mathematics, 56100 Siirt, Turkey.*

Received 24 March 2022; received in revised form 30 May 2022; accepted 18 October 2022

KEYWORDS
Variable heat flux;
Slip effect;
Viscous dissipation;
Heat generation;
FEM.

Abstract. The current study proposes an efficient numerical method to evaluate the effects of the variable heat flux, viscous dissipation, and slip velocity on the viscous Casson Heat Transfer (CHT), considering the unsteady stretching sheet that took into account the effect of heat generation or absorption. In this respect, Finite Element Method (FEM) was employed to solve the resulting ODEs that described the problem. The effects of the factors governing the HT such as unsteadiness parameter, slip velocity parameter, Casson parameter, local Eckert number, heat generation parameter, and Prandtl number were studied. In addition, the local skin friction coefficient and local Nusselt number on the stretching sheet were also computed. Finally, the obtained solutions confirmed that the proposed procedure could be an easy and efficient tool for finding a solution to such fluid models.

1. Introduction

Heat Transfer (HT) resulting from unsteady stretching sheet has attracted ever-increasing research interest owing to its numerous practical applications in various manufacturing processes and technology since Crane [1] presented an analytical solution for the model of steady flow for a Newtonian fluid deduced by a stretched flat sheet which moved through its plane at a velocity varying linearly in the range of fixed points. The problem posed by Crane [1] was then extended, taking into account a porous sheet by Gupta et al. [2], obtained an exact solution of the system under study. Grubka and Bobba [3] investigated the thermal field and came up with a solution to the energy equation using the properties of Kummer's functions. In the same field of study, a number of other relevant research studies have been carried out [4–17].

In nature, several fluid types can be classified as a Casson fluid that is marked by a purely viscous fluid with high viscosity. Some of the studies on this type of fluid may be found in [18–20]. Most of the previous studies have neglected the slip velocity condition at the boundary over a Stretching Surface (SS) while it is of importance in the case of obtaining the desired properties of the outcome. Many studies have been conducted and listed as [21–24] owing to the important applications of the HT characteristics in the case of slip effects over an SS.

Inspired by the former research, many researchers have successfully applied a variety of numerical methods in this field [25–28] among which the Finite Element Method (FEM) is the most acknowledged one

*. *Corresponding author.*
E-mail address: minc@firat.edu.tr (M. Inc)

doi: 10.24200/sci.2022.60176.6644

[29,30] owing to its advantages that help solve this class of equations where the solution coefficients can be easily obtained through any one of the numerical programs. For this reason, FEM was found to be much faster than other methods. Kochnev [31] investigated the FEM for atoms. Zhang and Cu [32] explored the condensed generalized finite element method in detail. Tolle and Marheineke [33] presented the extended finite element method. Bertrand et al. [34] discussed the robust and reliable finite element methods in poromechanics.

Nevertheless, the motivation behind this study was to employ an extensively validated, highly efficient, and variational finite element code to study the Casson fluid flow over a USS with internal heat generation, viscous dissipation, and variable heat flux involving Boundary Conditions (BCs) of slip effect. This investigation will be of immediate interest to all those processes that are highly affected by the heat enhancement concept, e.g., the inflow of blood through the industrial artery, which can be polished by a material governing the blood flow. In this study, FEM was used to numerically solve the normalized boundary layer equations to examine the effects of the following parameters and coefficients on the relevant flow variables in detail:

M Magnetic variable
β Casson variable
S Unsteady variable
m Time indices variable
r Space indices variable
γ Local heat generation/absorption variable
λ Velocity slip variable
Pr Prandtl number
Ec Local Eckert number

This study is organized as follows. A full description of the problem is given in Section 2. The procedure of finding the solution through the finite element method is discussed in Section 3. The numerical simulations are performed and explained in Section 4. Finally, the concluding remarks are given in Section 5.

2. Description of the problem

Consider an electrically Casson fluid flowing unpredictably through an extending horizontal impermeable sheet. Along the y-axis, a strong magnetic field is imposed (Figure 1). Because the magnetic Reynolds number of the flow is assumed to be very small, the induced magnetic field is ignored. We also suppose that the fluid is subjected to heat generation and heat flux, and that all fluid properties remain constant.

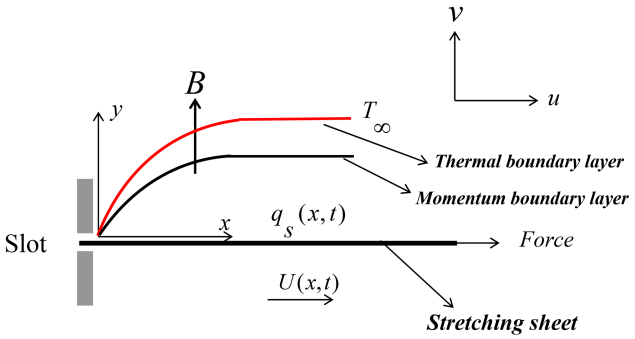

Figure 1. Schematic diagram of the problem.

The x and y axes were considered to be along and perpendicular to the plane of the sheet, respectively. Suppose that:

$$U = \frac{cx}{1-\alpha t}. \tag{1}$$

Here, we need to show that the shape of the sheet velocity in Eq. (1) is held only for times $t < \alpha^{-1}$ unless $\alpha = 0$. Then, consider [35]:

$$q_s(x,t) = -\kappa \frac{\partial T}{\partial y} = T_0 \frac{dx^r}{(1-\alpha t)^{m+\frac{1}{2}}}, \tag{2}$$

where κ is the fluid thermal conductivity; T and T_0 are the temperature and reference temperature of the fluid, respectively; and d is a fixed number. Now, the state for an incompressible flow of a Casson fluid is described by the following rheological equation [36–38]:

$$\tau_{ij} = \begin{cases} 2(\mu_B + P_y/\sqrt{2\pi})e_{ij}, & \pi > \pi_c \\ 2(\mu_B + P_y/\sqrt{2\pi_c})e_{ij}, & \pi < \pi_c \end{cases}$$

The heat generation/absorption term Q can be obtained as [38]:

$$Q = \begin{cases} Q_0(T - T_\infty), & T \geq T_\infty, \\ 0, & T < T_\infty. \end{cases} \tag{3}$$

For this kind of flow, we have [39]:

$$\frac{\partial u}{\partial x} + \frac{\partial v}{\partial y} = 0, \tag{4}$$

$$\frac{\partial u}{\partial t} + u\frac{\partial u}{\partial x} + v\frac{\partial u}{\partial y} = \nu(1+\frac{1}{\beta})\frac{\partial^2 u}{\partial y^2} - \frac{\sigma B_0^2}{\rho}u, \tag{5}$$

$$\frac{\partial T}{\partial t} + u\frac{\partial T}{\partial x} + v\frac{\partial T}{\partial y} = \frac{\kappa}{\rho c_p}\frac{\partial^2 T}{\partial y^2} + \frac{\nu}{c_p}(1+\frac{1}{\beta})\left(\frac{\partial u}{\partial y}\right)^2 + \frac{Q_0}{\rho c_p}(T - T_\infty), \tag{6}$$

where u and v are the velocity components, ρ is the fluid density, $\beta = \mu_B\sqrt{2\pi_c}/P_y$ is the Casson variable. The suitable BCs can be represented as:

$$u = U(x,t) + N_1\left(1+\frac{1}{\beta}\right)\frac{\partial u}{\partial y}, \qquad v = 0,$$

$$-\kappa\frac{\partial T}{\partial y} = q_s(x,t), \quad \text{at} \quad y = 0, \tag{7}$$

$$u \to 0, \quad T \to T_\infty, \quad \text{as} \quad y \to \infty. \tag{8}$$

It is critical to point out that the first part of Eq. (7) represents the slip velocity phenomenon. Physically, this phenomenon has significant technological applications such as polishing artificial heart valves and interior cavities, to name a few [24,40]. Here, $N_1 = N(1-\alpha t)^{\frac{1}{2}}$ is the velocity slip factor which changes with time, and N the initial value of velocity factor. Likewise, the third part of Eq. (7) is utilized to determine the rate of heat transfer, which is essential for the cooling process [41]. The mathematical formulation of the model can be simplified by inserting the following dimensionless coordinates:

$$\eta = (\frac{c}{\nu})^{\frac{1}{2}}(1-\alpha t)^{\frac{-1}{2}}y, \qquad u = \frac{cx}{1-\alpha t}f'(\eta),$$

$$v = -\frac{\sqrt{c\nu}}{(1-\alpha t)^{\frac{1}{2}}}f(\eta), \tag{9}$$

$$T = T_\infty + T_0(\frac{dx^r}{\kappa\sqrt{c/\nu}})(1-\alpha t)^{-m}\theta(\eta). \tag{10}$$

Eqs. (9)–(10) are valid only for $\alpha t \ll 1$, where $f(\eta)$ is the dimensionless stream function and $\theta(\eta)$ is the dimensionless temperature.

Based on the last two equations, the mathematical problem defined in Eqs. (5)–(8) will be reduced to a collection of ODEs and their associated boundary conditions, as shown below:

$$\left(1+\frac{1}{\beta}\right)f''' + ff'' - f'^2 - \frac{\eta}{2}Sf'' - (S+M)f' = 0, \tag{11}$$

$$\frac{1}{Pr}\theta'' + f\theta' - rf'\theta - \frac{\eta}{2}S\theta' + Ec\left(1+\frac{1}{\beta}\right)f''^2 - (Sm-\gamma)\theta = 0, \tag{12}$$

$$f = 0, \qquad f' = 1 + \lambda\left(1+\frac{1}{\beta}\right)f'', \qquad \theta' = -1,$$

$$\text{at} \qquad \eta = 0, \tag{13}$$

$$f' \to 0, \quad \theta \to 0, \qquad \text{as} \qquad \eta \to \infty, \tag{14}$$

where a prime denotes differentiation w.r.t. η $S = \frac{\alpha}{c}$; is the unsteadiness parameter; $Ec = \frac{U^2}{c_p\Delta T}$; $\Delta T = T_0(\frac{dx^r}{\kappa\sqrt{c/\nu}})(1-\alpha t)^{-m}$; $\gamma = \frac{xQ_0}{U\rho c_p}$ is the native heat generation (> 0) or absorption (< 0) parameter; and $Pr = \frac{\rho\nu c_p}{\kappa}$.

In engineering and practical applications, our interest lies in the realization of the paramount physical parameters of the flow behavior and HT characteristics by analyzing Cf_x and Nu_x. These non-dimensional parameters are defined as:

$$Cf_x = -2Re_x^{\frac{-1}{2}}\left(1+\frac{1}{\beta}\right)f''(0), \quad Nu_x = \frac{Re_x^{\frac{1}{2}}}{\theta(0)}, \tag{15}$$

where $Re_x = \frac{Ux}{\nu}$ is the local Reynolds number.

3. Procedure of solution by the FEM

FEM is a powerful method for the numerical treatment of the differential equations, taking into consideration the basic assumption that the whole domain is divided into **Finite Elements**. In addition, this method is a versatile numerical procedure used for solving many different problems such as fluid mechanics [42], heat transfer [43], etc. FEM is implemented through the following steps [44]:

1. *Finite-element discretization:* The finite-element mesh is constructed by a collection of these elements.
2. *Element equations derivation:*
   - Construct the Variational Formulation (VF) of the presented problem for all typical elements isolated from the proposed mesh;
   - Assume an approximate solution of the VF and, then, substitute it with the element equations;
   - Construct the stiffness matrix (the element matrix) in terms of element interpolation functions.
3. *Element equations collection:* Collect the algebraic equations to obtain a large number of algebraic equations.
4. *BCs insertion:* Insert the essential and natural BCs into the collected equations.
5. *Algebraic equations solving:* Assess the set of algebraic equations using any of the suitable numerical techniques.

The solutions to the simultaneous ODEs, as given in Eqs. (11) and (12) with the BCs (Eqs. (13) and (14)), will be obtained through the following steps:

Suppose that $f'(\eta) = h(\eta)$. Then, the set of Eqs. (11)–(12) will be:

$$f' - h = 0, \tag{16}$$

$$\left(1+\frac{1}{\beta}\right)h'' + fh' - h^2 - 0.5S\eta h' - (S+M)h = 0, \tag{17}$$

$$\frac{1}{Pr}\theta'' + f\theta' - rh\theta - 0.5S\eta\theta' + Ec\left(1+\frac{1}{\beta}\right)h'^2 + (\gamma - Sm)\theta = 0. \quad (18)$$

The corresponding BCs in the bounded domain $(0, \eta_\infty)$ are obtained as:

$$f(0) = 0, \qquad h(0) = 1 + \lambda\left(1+\frac{1}{\beta}\right)f'(0),$$

$$\theta'(0) = -1, \quad (19)$$

$$h \to 0, \quad \theta \to 0, \qquad \text{as} \qquad \eta \to \infty. \quad (20)$$

3.1. Variational formulation

The variational form associated with Eqs. (16)–(18) over a typical linear element (η_e, η_{e+1}), can be constructed:

$$\int_{\eta_e}^{\eta_{e+1}} \phi_1[f' - h]d\eta, \quad (21)$$

$$\int_{\eta_e}^{\eta_{e+1}} \phi_2[(1+\beta^{-1})h'' + fh' - h^2 - 0.5\,S\eta h' - (S+M)h]d\eta, \quad (22)$$

$$\int_{\eta_e}^{\eta_{e+1}} \phi_3\left[\frac{1}{Pr}\theta'' + f\theta' - rh\theta - 0.5S\eta\,\theta' + Ec(1+\beta^{-1})h'^2 + (\gamma - Sm)\theta\right]d\eta, \quad (23)$$

where ϕ_1, ϕ_2, and ϕ_3 are the arbitrary test functions that may be observed as the variation of f, h, and θ.

3.2. Finite element formulation

We have:

$$f(\eta) = \sum_{\ell=1}^{2} f_\ell \Upsilon_\ell, \qquad h(\eta) = \sum_{\ell=1}^{2} h_\ell \Upsilon_\ell,$$

$$\theta(\eta) = \sum_{\ell=1}^{2} \theta_\ell \Upsilon_\ell, \quad (24)$$

with $\phi_1 = \phi_2 = \phi_3 = \Upsilon_\ell$, and $\ell = 1, 2$.

In our calculations, the shape functions for a typical element (η_e, η_{e+1}) are chosen by:

Linear element:

$$\Upsilon_1^e = \frac{\eta_{e+1} - \eta}{\eta_{e+1} - \eta_e}, \qquad \Upsilon_2^e = \frac{\eta - \eta_e}{\eta_{e+1} - \eta_e},$$

$$\eta_e \le \eta \le \eta_{e+1}. \quad (25)$$

Quadratic element:

$$\Upsilon_1^e = \frac{(\eta_{e+1} - \eta_e - 2\eta)(\eta_{e+1} - \eta)}{(\eta_{e+1} - \eta_e)^2},$$

$$\Upsilon_2^e = \frac{4(\eta - \eta_e)(\eta_{e+1} - \eta)}{(\eta_{e+1} - \eta_e)^2},$$

$$\Upsilon_3^e = -\frac{(\eta_{e+1} - \eta_e - 2\eta)(\eta - \eta_e)}{(\eta_{e+1} - \eta_e)^2},$$

$$\eta_e \le \eta \le \eta_{e+1}. \quad (26)$$

The FEM of the formed equations can be described by:

$$\begin{pmatrix} [K^{11}] & [K^{12}] & [K^{13}] \\ [K^{21}] & [K^{22}] & [K^{23}] \\ [K^{31}] & [K^{32}] & [K^{33}] \end{pmatrix} \begin{pmatrix} [f] \\ [h] \\ [\theta] \end{pmatrix} = \begin{pmatrix} [b^1] \\ [b^2] \\ [b^3] \end{pmatrix}, \quad (27)$$

where $[K^{rs}]$ and $[b^r]$ $(r, s = 1, 2, 3)$ are interpreted as:

$$K_{ij}^{11} = \int_{\eta_e}^{\eta_{e+1}} \left(\Upsilon_i \frac{d\Upsilon_j}{d\eta}\right)d\eta,$$

$$K_{ij}^{12} = -\int_{\eta_e}^{\eta_{e+1}} (\Upsilon_i \Upsilon_j)\,d\eta, \qquad K_{ij}^{13} = 0,$$

$$K_{ij}^{21} = \int_{\eta_e}^{\eta_{e+1}} \left(\Upsilon_i \frac{d\Upsilon_j}{d\eta}\right)d\eta, \qquad K_{ij}^{23} = 0,$$

$$K_{ij}^{22} = -\int_{\eta_e}^{\eta_{e+1}} \left[(1+\beta^{-1})\left(\frac{d\Upsilon_i}{d\eta}\frac{d\Upsilon_j}{d\eta}\right) - \left(0.5S\Upsilon_i\frac{d\Upsilon_j}{d\eta} + (S+M)\Upsilon_i\Upsilon_j\right)\right]d\eta - \int_{\eta_e}^{\eta_{e+1}} \left(\Upsilon_i \bar{h} \Upsilon_j\right)d\eta,$$

$$K_{ij}^{31} = \int_{\eta_e}^{\eta_{e+1}} \left(\Upsilon_i \bar{\theta}' \Upsilon_j\right)d\eta,$$

$$K_{ij}^{32} = -r\int_{\eta_e}^{\eta_{e+1}} \left(\Upsilon_i \bar{\theta} \Upsilon_j\right)d\eta + Ec\left(1+\beta^{-1}\right)\int_{\eta_e}^{\eta_{e+1}} \left(\Upsilon_i \bar{h}' \frac{d\Upsilon_j}{d\eta}\right)d\eta,$$

$$K_{ij}^{33} = \int_{\eta_e}^{\eta_{e+1}} \left[\left(\frac{1}{Pr}\right) \left(\frac{d\Upsilon_i}{d\eta}\frac{d\Upsilon_j}{d\eta}\right) - 0.5\ Sm \left(\Upsilon_i \frac{d\Upsilon_j}{d\eta}\right) + (\gamma - Sm)\left(\Upsilon_i \Upsilon_j\right) \right] d\eta,$$

$$b_i^1 = 0, \qquad b_i^2 = -\left(1+\beta^{-1}\right)\left(\Upsilon_i \frac{dh}{d\eta}\right)_{\eta_e}^{\eta_{e+1}},$$

$$b_i^3 = -\left(\frac{1}{Pr}\right)\left(\Upsilon_i \frac{dh}{d\eta}\right)_{\eta_e}^{\eta_{e+1}}, \tag{28}$$

where:

$$\bar{h} = \sum_{\ell=1}^{2} \bar{h_\ell} \Upsilon_\ell, \qquad \bar{h'} = \sum_{\ell=1}^{2} \bar{h_\ell} \frac{d\Upsilon_\ell}{d\eta},$$

$$\bar{\theta} = \sum_{\ell=1}^{2} \bar{\theta_\ell} \Upsilon_\ell, \qquad \bar{\theta'} = \sum_{\ell=1}^{2} \bar{\theta_\ell} \frac{d\Upsilon_\ell}{d\eta}.$$

4. Numerical simulation

The estimated value of the wall temperature $\theta(0)$ of for different values of the Prandtl number Pr was compared with those obtained by Prasad et al. [45] to examine the accuracy of the proposed numerical method. According to the results listed in Table 1, our findings are in good agreement with the findings already published in the literature.

This section discusses the conduct of the physical parameters governing the proposed model namely M, β, S, m, r, γ, λ, Pr and Ec. These physical parameters are used in the range of $0.0 \leq M \leq 0.9$, $0.0 \leq S \leq 1.4$, $0.2 \leq \beta \leq \infty$, $0.0 \leq \lambda \leq 1.0$, $0.7 \leq Pr \leq 2.0$, $0.0 \leq Ec \leq 0.9$, $1.0 \leq m \leq 4.0$, $-1.0 \leq \gamma \leq 1.0$ and $1.0 \leq r \leq 4.0$ [39]. As a result, the values of the parameters with fixed values are displayed graphically as $M = \lambda = 0.2$, $Pr = 1.3$, $Ec = 0.2$, $r = m = 2.0$, $\beta = 0.5$, and $S = 0.8$. Figure 2(a) and (b) examine the influence of magnetic number M on the velocity and temperature profiles respectively. Figure 2(a) exhibits that the velocity is a decreasing function of M, whereas Figure 2(b) is an increasing function of the same parameter M.

Table 1. Comparison of wall temperature $\theta(0)$ with the results obtained by Prasad et al. [45] (Newtonian case) when $M = 1, \lambda = S = 0, r = 1, Ec = 0$, and $\beta \to \infty$.

Pr	Prasad et al. [45]	Present work
0.7	1.3755	1.37549852
1.0	1.0993	1.09927985
2.0	0.7066	0.70655958
5.0	0.4087	0.40868792
10.0	0.2776	0.27759875

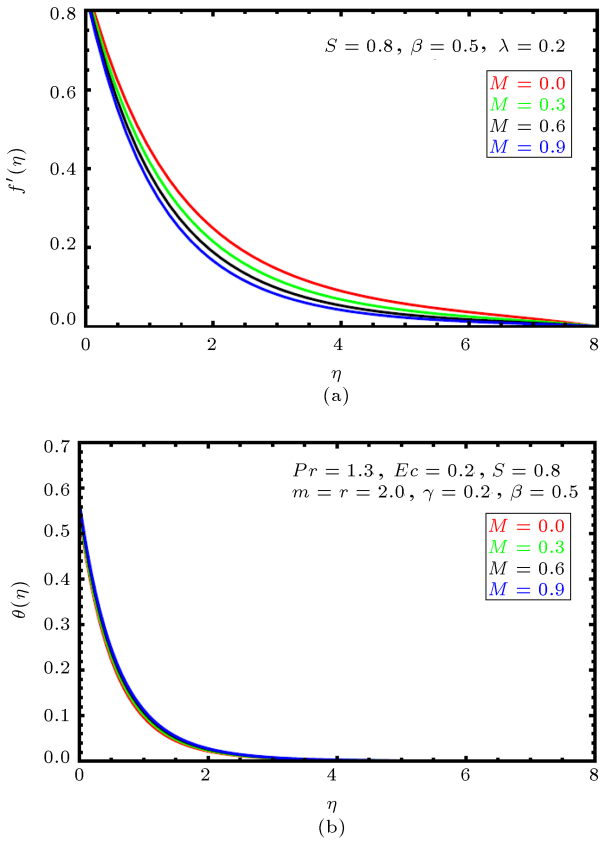

Figure 2. (a) Velocity profiles for M. (b) Temperature profiles for M.

Figure 3(a) is plotted to examine the dimensionless velocity profiles inside Boundary Layer (BL) for different values of S. As observed in this figure, increase in the value of the unsteadiness parameter leads to a fall in the flow velocity profiles inside the BL. In addition, under the effect of heat flux along the sheet, the temperature profiles along the BL and wall temperature $\theta(0)$ decrease upon increasing the same parameter (Figure 3(b)) and the cooling rate at higher values of S is quite high while it decreases at smaller values of S.

Figure 4(a) shows the velocity profiles versus the similarity variable η for different values of β. As observed, an increase in β value leads to an increase in the velocity profiles along the sheet; however, the reverse is true away from the sheet. In addition, the thickness of the BL decreases upon increasing β. Figure 4(b) depicts the temperature profiles for different values of the same parameter according to which both the temperature in the thermal BL and wall temperature $\theta(0)$ increase followed by increasing the Casson parameter but in weakly differences between values of the same parameter.

Figure 5(a) and (b) show the effect of γ on the velocity and temperature profiles. As observed in Figure 5(a), both velocity profiles inside the BL and

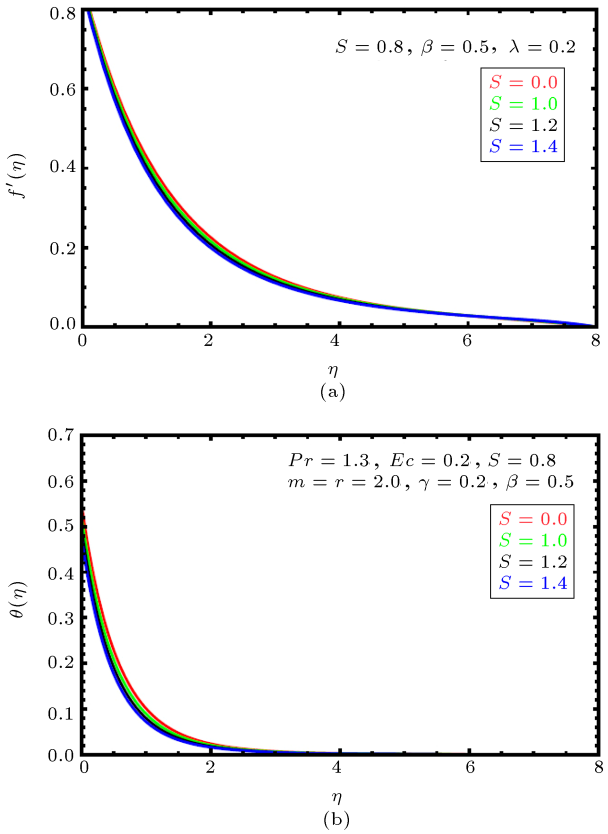

Figure 3. (a) Velocity profiles for S. (b) Temperature profiles for S.

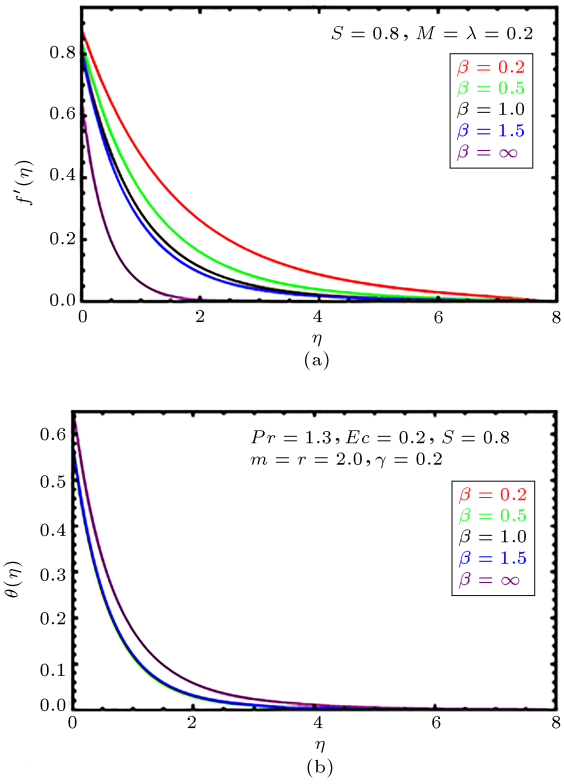

Figure 4. (a) Velocity description for β. (b) Temperature description for β.

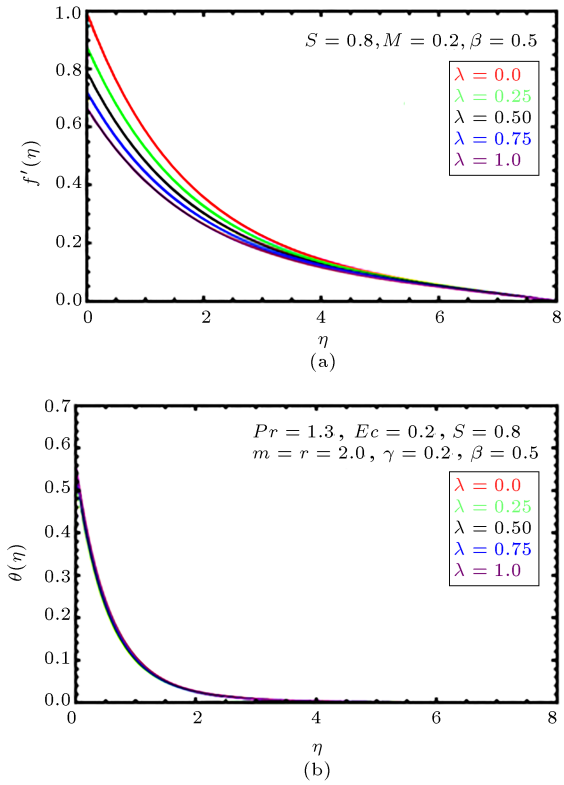

Figure 5. (a) Velocity description for λ. (b) Temperature description for λ.

BL thickness decrease as the slip velocity parameter increases. Physically, under the slip condition, the slipping fluid reduces the surface skin friction values between the fluid and stretching sheet. As a result, increasing the value of the slip velocity parameter will reduce the flow velocity in the region of the BL. The dimensionless temperature profiles within the BL region for the slip velocity parameter are illustrated in Figure 5(b) according to which any increase in γ may result in an increase in both wall temperature $\theta(0)$ and the fluid temperature profiles in the thermal BL.

Figure 6(a) graphically shows the effect of the Prandtl number, Pr, on the temperature distribution above the sheet. In this figure, a decrease in the Pr may result in increase in the thermal BL thickness, temperature profiles, and temperature of the wall $\theta(0)$ mainly because the higher values of the Prandtl number correspond to the weaker thermal diffusivity. Clearly, the Prandtl number has a direct effect on the temperature field, as shown by the governing equations (Eqs. (11)-(14)); however, it does not affect the fluid velocity field. For this reason, changing the Prandtl number values did not affect the fluid velocity distributions. Figure 6(b) elaborates the effect of the Eckert number on the temperature profile. Evidently, the effect of increasing Eckert number Ec will increase both the temperature profiles along the BL and surface temperature $\theta(0)$. This is, of course, a consequence

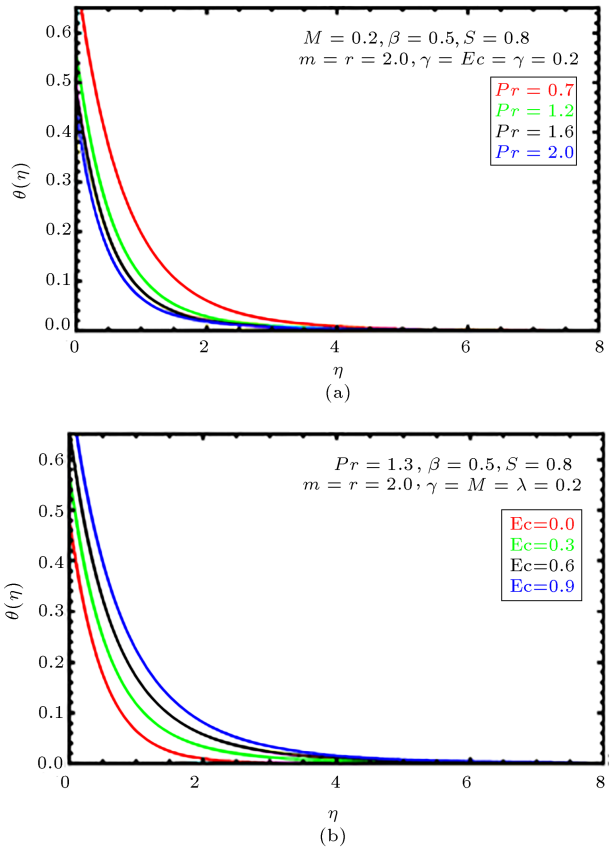

Figure 6. (a) Temperature description for Pr. (b) Temperature description for Ec.

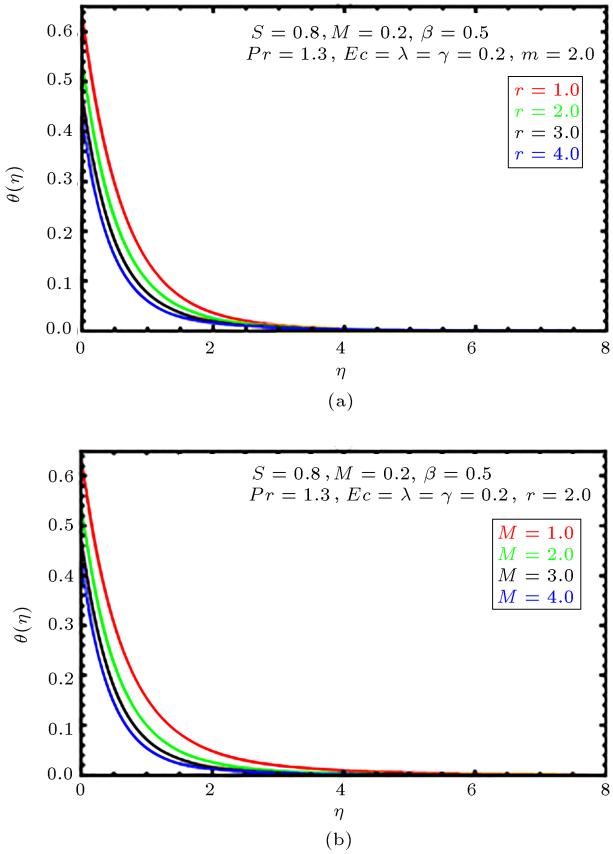

Figure 7. (a) Temperature description for r (b). Temperature description for m.

of the fact that at higher values of the Ec, there is significant heat generation due to viscous dissipation near the sheet. In this regard, viscous dissipation in a flow due to a stretching sheet is beneficial to providing the required temperature.

Figure 7(a) and (b) illustrate how temperature profiles are affected by the change in the space index parameter r or (the time index parameter m) when other parameters remain fixed. These figures indicate that the dimensionless temperature profile turns depressed following increase in the values of the two parameters. Likewise, the effect of increasing these two parameters will cause a decline in the temperature of the wall $\theta(0)$.

Moreover, Figure 8 illustrates how temperature profiles are affected by the variations in the heat generation/absorption parameter γ when other parameters remain constant. This figure also indicates that the thermal BL thickness values increase when $\gamma > 0$ becomes stronger, while the opposite effect can be observed when $\gamma < 0$. In addition, the highest temperature behavior for the fluid in the BL was obtained with the greatest heat generation parameters $\gamma > 0$. Likewise, the effect of heat absorption parameters $\gamma < 0$ causes a drop in the temperature profiles as the heat dissipated from the sheet is absorbed.

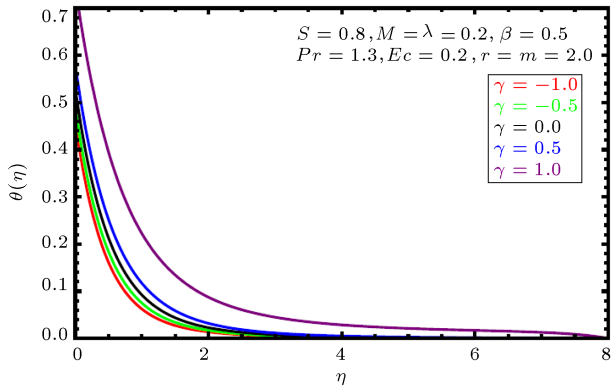

Figure 8. Temperature description for γ.

Table 2 shows the effect of different values of physical governing parameters of M, β, S, m, r, Pr, λ and Ec, all required for the evaluation $-(1+\frac{1}{\beta})f''(0)$ and $\frac{1}{\theta(0)}$. Of note, an increase in the value of the unsteady parameter causes an increase in both Cf_x and Nu_x. In addition, the local Cf_x decreases by increasing β while Nu_x increases by increasing the values. With an increase in λ both the local Cf_x and Nu_x are reduced. In addition, any increase in the values of Ec and γ leads to a decrease in Nu_x. Further, an increase in the Pr will increase Nu_x value, mainly because

Table 2. Variation of $-(1+\frac{1}{\beta})f''(0)$ and $\frac{1}{\theta(0)}$ for distinct values of $M, S, \beta, \lambda, \gamma, Ec, r, m$ and Pr.

M	S	β	λ	Pr	Ec	r	m	γ	$-(1+\frac{1}{\beta})f''(0)$	$\frac{1}{\theta(0)}$
0.0	0.8	0.5	0.2	1.3	0.2	2.0	2.0	0.2	1.42101	1.78389
0.2	0.8	0.5	0.2	1.3	0.2	2.0	2.0	0.2	1.48953	1.76116
0.5	0.8	0.5	0.2	1.3	0.2	2.0	2.0	0.2	1.58118	1.73096
0.2	0.8	0.5	0.2	1.3	0.2	2.0	2.0	0.2	1.48975	1.76104
0.2	1.0	0.5	0.2	1.3	0.2	2.0	2.0	0.2	1.53819	1.86843
0.2	1.0	0.5	0.2	1.3	0.2	2.0	2.0	0.2	1.58376	1.97008
0.2	1.4	0.5	0.2	1.3	0.2	2.0	2.0	0.2	1.62672	2.06688
0.2	0.8	0.2	0.2	1.3	0.2	2.0	2.0	0.2	1.84905	1.74277
0.2	0.8	0.5	0.2	1.3	0.2	2.0	2.0	0.2	1.48953	1.76116
0.2	0.8	1.0	0.2	1.3	0.2	2.0	2.0	0.2	1.29823	1.76601
0.2	0.8	1.5	0.2	1.3	0.2	2.0	2.0	0.2	1.21724	1.76669
0.2	0.8	0.5	0.0	1.3	0.2	2.0	2.0	0.2	2.31847	1.83242
0.2	0.8	0.5	0.5	1.3	0.2	2.0	2.0	0.2	0.99485	1.66516
0.2	0.8	0.5	1.0	1.3	0.2	2.0	2.0	0.2	0.65078	1.56523
0.2	0.8	0.5	0.2	0.8	0.2	2.0	2.0	0.2	1.48953	1.38704
0.2	0.8	0.5	0.2	1.3	0.2	2.0	2.0	0.2	1.48953	1.76116
0.2	0.8	0.5	0.2	2.0	0.2	2.0	2.0	0.2	1.48953	2.16256
0.2	0.8	0.5	0.2	1.3	0.0	2.0	2.0	0.2	1.48953	1.86381
0.2	0.8	0.5	0.2	1.3	0.2	2.0	2.0	0.2	1.48953	1.76116
0.2	0.8	0.5	0.2	1.3	0.5	2.0	2.0	0.2	1.48953	1.62677
0.2	0.8	0.5	0.2	1.3	0.2	1.0	2.0	0.2	1.48953	1.54332
0.2	0.8	0.5	0.2	1.3	0.2	2.0	2.0	0.2	1.48953	1.76116
0.2	0.8	0.5	0.2	1.3	0.2	3.0	2.0	0.2	1.48953	1.96055
0.2	0.8	0.5	0.2	1.3	0.2	2.0	1.0	0.2	1.48953	1.44167
0.2	0.8	0.5	0.2	1.3	0.2	2.0	2.0	0.2	1.48953	1.76116
0.2	0.8	0.5	0.2	1.3	0.2	2.0	1.0	0.2	1.48953	2.02621
0.2	0.8	0.5	0.2	1.3	0.2	2.0	2.0	-1.0	1.48953	2.14588
0.2	0.8	0.5	0.2	1.3	0.2	2.0	2.0	-0.5	1.48953	1.99512
0.2	0.8	0.5	0.2	1.3	0.2	2.0	2.0	0.0	1.48953	1.83129
0.2	0.8	0.5	0.2	1.3	0.2	2.0	2.0	0.5	1.48953	1.64976
0.2	0.8	0.5	0.2	1.3	0.2	2.0	2.0	1.0	1.48953	1.44167

a fluid with a higher value of Pr possesses a large heat capacity, thus intensifying the HT. Finally, Nu_x increases as the space index parameter, heat absorption parameter, and time index parameter increase in value.

5. Conclusions

The BL heat transfer of a Casson fluid over an unsteady stretching sheet with slip effects, viscous dissipation, variable heat flux, and internal heat generation/absorption was analyzed in this study.

The governing PDEs were converted into the ODEs using a suitable dimensionless transformation which were numerically treated by appointing the FEM. According to the results, increasing the values of S, heat absorption parameter, or the Pr would lead to an increase in Nu_x. In addition, Cf_x and Nu_x values decreased upon increasing λ. Further, the fluid temperature rose followed by increasing the magnetic number and Eckert parameters. Likewise, both higher values of the slip velocity parameter or Casson parameter caused a decrease in the velocity

profile. Finally, it was observed that the Nu_x decreased as both the heat generation parameter or the Ec increased; however, the opposite was true for β. In addition, as the time index parameter or space index parameter increased in magnitude, Nu_x value was elevated.

References

1. Crane, L.J. "Flow past a stretching plate", *Zeitschrift für Angewandte Mathematik und Physik*, **21**, pp. 645–647 (1970)
2. Gupta, P.S. and Gupta, A.S. "Heat and mass transfer on a stretching sheet with suction or blowing", *Can. J. Chem. Eng.*, **55**, pp. 744–746 (1977).
3. Grubka, L.J. and Bobba, K.M. "Heat transfer characteristics of a continuous stretching surface with variable temperature", *ASME J. Heat Transfer*, **107**, pp. 248–250 (1985).
4. Ali, A., Hussain, M., Anwar, M.S., et al. "Mathematical modeling and parametric investigation of blood flow through a stenosis artery", *Applied Mathematics and Mechanics*, **42**, pp. 1675-1684 (2021).
5. Hussain, Z., Hayat, T., Alsaedi, A., et al. "Mixed convective flow of CNTs nanofluid subject to varying viscosity and reactions", *Scientifc Reports*, **11**, pp. 1–14 (2021).
6. Irfan, M., Rafiq, K., Anwar, M.S., et al. "Evaluating the performance of new mass flux theory on Carreau nanofluid using the thermal aspects of convective heat transport", *Pramana*, **95**, pp. 1–15 (2021).
7. Ali, I., Rasheed, A., Anwar, M.S., et al. "Fractional calculus approach for the phase dynamics of Josephson junction", *Chaos, Solitons & Fractals*, **143**, p. 110572 (2021).
8. Hussain, Z., Hussain, A., Anwar, M.S., et al. "Analysis of Cattaneo-Christov heat flux in Jeffery fluid flow with heat source over a stretching cylinder", *Journal of Thermal Analysis and Calorimetry*, **147**, pp. 3391–3402 (2022).
9. Hussain, Z., Muhammad, S., and Anwar, M.S. "Effects of first-order chemical reaction and melting heat on hybrid nanoliquid flow over a nonlinear stretched curved surface with shape factors", *Advances in Mechanical Engineering*, **13**(4), pp. 1–12 (2021).
10. Irfan, M., Rafiq, M.K., Waqas, M., et al. "Theoretical analysis of new mass flux theory and Arrhenius activation energy in Carreau nanofluid with magnetic influence", *International Communications in Heat and Mass Transfer*, **120**, pp. 105051 (2021).
11. Khan, K.A., Butt, A.R., Raza, N., et al. "Unsteady magneto-hydrodynamics flow between two orthogonal moving porous plates", *The European Physical Journal Plus*, **134**, pp. 1–16 (2019).
12. Bayones, F.S., Nisar, K.S., Khan, K.A., et al. "Magneto-hydrodynamics (MHD) flow analysis with mixed convection moves through a stretching surface", *AIP Advances*, **11**, pp. 1–8 (2021).
13. Khan, K.A., Seadawy, A.R., and Jhangeer, A. "Numerical appraisal under the influence of the time dependent Maxwell fluid flow over a stretching sheet", *Mathematical Methods in the Applied Sciences*, **44**(7), pp. 5265–5279 (2021).
14. Khan, K.A., Butt, A., and Raza, N. "Influence of porous medium on magneto hydrodynamics boundary layer flow through elastic sheet with heat and mass transfer", *J. Nanofluids*, **8**(4), pp. 725–735 (2019).
15. Seadawy, A.R., Raza, N., Khalil, O.H., et al. "Computational approach and flow analysis of chemically reactive tangent hyperbolic nanofluid over a cone and plate", *Waves in Random and Complex Media* (2021). https://DOI.org/10.1080/17455030.2021.1959960
16. Khan, K.A., Jamil, F., Ali, J., et al. "Analytical simulation of heat and mass transmission in Casson fluid flow across a stretching surface", *Mathematical Problems in Engineering*, **2022**, p. 5576194 (2022).
17. Aly, K., Seadawy, A.R., and Raza, N. "The homotopy simulation of MHD time dependent three-dimensional shear thinning fluid flow over a stretching plate", *Chaos Solitons & Fractals*, **157**, p. 111888 (2022).
18. Bhattacharyya, K., Hayat, T., and Alsaedi, A. "Exact solution for boundary layer flow of Casson fluid over a permeable stretching/shrinking sheet", *ZAMM Z. Angew. Math. Mech.*, **94**, pp. 522–528 (2014).
19. Mukhopadhyay, S., Ranjan De, P., Bhattacharyya, K., and Layek, G.C. "Casson fluid flow over an unsteady stretching surface", *Ain Shams Engineering Journal*, **4**, pp. 933–938 (2013).
20. Boyd, J., Buick, J.M., and Green, S. "Analysis of the Casson and Carreau-Yasuda non-Newtonian blood models in steady and oscillatory flow using the lattice Boltzmann method", *Phys Fluids*, **19**, pp. 93–103 (2007).
21. Thompson, P.A. and Troian, S.M. "A general boundary condition for liquid flow at solid surfaces", *Nature*, **389**, pp. 360–362 (1997).
22. Megahed, A.M. "HPM for slip velocity effect on a liquid film over an unsteady stretching surface with variable heat flux", *The European Physical Journal Plus*, **126**, pp. 1–8 (2011).
23. Turkyilmazoglu, M. "Multiple solutions of heat and mass transfer of MHD slip flow for the viscoelastic fluid over a stretching sheet", *Inter. J. Thermal Sciences*, **50**, pp. 2264–2276 (2011).
24. Megahed, A.M. "Variable viscosity and slip velocity effects on the flow and heat transfer of a power-law fluid over a non-linearly stretching surface with heat flux and thermal radiation", *Rheologica Acta*, **51**, pp. 841–847 (2012).
25. Khader, M.M. and Saad, K.M. "A numerical study using Chebyshev collocation method for a problem of biological invasion: fractional Fisher equation", *Int. J. Biomathematics*, **11**(8), pp. 1–15 (2018).

26. Khader, M.M. and Saad, K.M. "On the numerical evaluation for studying the fractional KdV, KdV-Burger's, and Burger's equations", *European Physical Journal Plus*, **133**, pp. 1–13 (2018).
27. Khader, M.M. and Saad, K.M. "A numerical approach for solving the problem of biological invasion (fractional Fisher equation) using Chebyshev spectral collocation method", *Chaos, Solitons & Fractals*, **110**, pp. 169–177 (2018).
28. Saad, K.M., Khader, M.M., Gomez-Aguilar, J.F., and Baleanu, D., "Numerical solutions of the fractional Fisher's type equations with Atangana-Baleanu fractional derivative by using spectral collocation methods", *Chaos*, **29**, pp. 1–5 (2019).
29. Khader, M.M. "The numerical solution for BVP of the liquid film flow over an unsteady stretching sheet with thermal radiation and magnetic field using the finite element method", *Int. J. Modern Physics C.*, **30**(11), pp. 1–8 (2019).
30. Khader, M.M. and Khadijah, M.A. "Galerkin-FEM for obtaining the numerical solution of the linear fractional Klein-Gordon equation", *J. Applied Analysis and Computation*, **9**(1), pp. 261–270 (2019).
31. Kochnev, V.K. "Finite element method for atoms", *Chemical Physics*, **548**(1), pp. 111197 (2021).
32. Zhang, Q. and Cu, C. "Condensed generalized finite element method", *Numerical Methods in Partial Differential Equations*, **37**, pp. 1847–1868 (2021).
33. Tolle, K. and Marheineke, N. "Extended group finite element method", *Applied Numerical Mathematics*, **162**, pp. 1–19 (2021).
34. Bertrand, F., Ern, A., and Radu, F.A. "Robust and reliable finite element methods in poromechanics", *Computers and Mathematics with Applications*, **91**(1), pp. 1–2 (2021) .
35. Megahed A.M. "Variable heat flux effect on MHD flow and heat transfer over an unsteady stretching sheet in the presence of thermal radiation", *Canadian J. of Physics*, **92**, pp. 86–91 (2014).
36. Shahmohamadi, H. "Analytic study on non-Newtonian natural convection boundary layer flow with variable wall temperature on a horizontal plate", *Meccanica*, **47**, pp. 1313–1323 (2012).
37. Mustafa, M., Hayat, T., Pop, I., et al. "Stagnation-point flow and heat transfer of a Casson fluid towards a stretching sheet", *Zeitschrift für Naturforschung A*, **67**, pp. 70–76 (2012).
38. Mostafa, A.A.M. "The effects of variable fluid properties on MHD Maxwell fluids over a stretching surface in the presence of heat generation/absorption", *Chemical Engineering Communications*, **198**, pp. 131–146 (2011).
39. Megahed, A.M. "Effect of slip velocity on Casson thin film flow and heat transfer due to an unsteady stretching sheet in the presence of variable heat flux and viscous dissipation", *Applied Mathematics and Mechanics*, **36**, pp. 1273–1284 (2015).
40. Megahed, A.M. "Improvement of heat transfer mechanism through a Maxwell fluid flow over a stretching sheet embedded in a porous medium and convectively heated", *Mathematics and Computers in Simulation*, **187**, pp. 97–109 (2021).
41. Megahed, A.M. "Carreau fluid flow due to nonlinearly stretching sheet with thermal radiation, heat flux, and variable conductivity", *Applied Mathematics and Mechanics*, **40**, pp. 1615-1624 (2019).
42. Bhargava, R., Sharma, S., Takhar, H.S., et al. "Numerical solutions for micropolar transport phenomena over a nonlinear stretching sheet", *Nonlinear Anal: Model. Cont.*, **12**, pp. 45–63 (2007).
43. Reddy J.N., *An Introduction to the Finite Element Method*, New York: McGraw-Hill Book Co (1985).
44. Rana, P. and Bhargava, R. "Flow and heat transfer of a nanofluid over a nonlinearly stretching sheet: A numerical study", *Commun. Nonlinear Sci. Numer. Simulat.*, **17**, pp. 212–226 (2012).
45. Prasad, K.V., Pal, D., and Datti, P.S. "MHD power-law fluid flow and heat transfer over a non-isothermal stretching sheet", *Commun. Nonlinear Sci. Numer. Simulat.*, **14**, pp. 2178–2189 (2009).

Biographies

Mohamed M. Khader is a Professor of Pure Mathematics at Benha University. His research interests are in the areas of numerical analysis and mathematical physics including numerical methods for nonlinear differential equations. He has published several research papers in reputed international journals of mathematical and engineering sciences.

Mustafa Inc is a Professor of Applied Mathematics at Firat University. He received his PhD degree in Applied Mathematics from Firat university in 2002. He has worked as a Full Professor at the Department of Mathematics at Firat University. His research interests include applied mathematics, solutions of differential equations, optical soliton, Lie symmetry, and conservation laws. He supervised many MSc and PhD students. He has published research articles in reputed international journals of mathematical and statistical sciences. He also is a referee and an editor of mathematical journals.

Ali Akgul is a Professor of Applied Mathematics at Siirt University. He is also the Head of the Mathematics Department. He has made a big contribution to fractional calculus and numerical methods. He has more than 250 research papers in highly accredited journals. He has given many talks as an invited speaker in many international conferences.